Research Article Vol. 30, No. 4 / 14 Feb 2022 / Optics Express 4748
Optics EXPRESS

Nonlinear microscopy using impulsive stimulated Brillouin scattering for high-speed elastography

BENEDIKT KRUG,[1,5] NEKTARIOS KOUKOURAKIS,[1,2,5,6] JOCHEN GUCK,[3] AND JÜRGEN CZARSKE[1,2,4,7]

[1]*Laboratory of Measurement and Sensor System Technique, TU Dresden, Helmholtzstrasse 18, 01069 Dresden, Germany*
[2]*Competence Center for Biomedical Computational Laser Systems (BIOLAS), TU Dresden, Dresden, Germany*
[3]*Max Planck Institute for the Science of Light, Staudtstraße 2, 91058 Erlangen, Germany*
[4]*Cluster of Excellence Physics of Life, TU Dresden, Dresden, Germany*
[5]*Equally contributed*
[6]*nektarios.koukourakis@tu-dresden.de*
[7]*juergen.czarske@tu-dresden.de*

Abstract: The impulsive stimulated Brillouin microscopy promises fast, non-contact measurements of the elastic properties of biological samples. The used pump-probe approach employs an ultra-short pulse laser and a cw laser to generate Brillouin signals. Modeling of the microscopy technique has already been carried out partially, but not for biomedical applications. The nonlinear relationship between pulse energy and Brillouin signal amplitude is proven with both simulations and experiments. Tayloring of the excitation parameters on the biologically relevant polyacrylamide hydrogels outline sub-ms temporal resolutions at a relative precision of <1%. Brillouin microscopy using the impulsive stimulated scattering therefore exhibits high potential for the measurements of viscoelastic properties of cells and tissues.

1. Introduction

Contrast is a crucial parameter in microscopy of biological samples. Commonly fluorescent contrast agents, providing molecular specific information with high spatio-temporal resolution, are used in modern microscopes. However, these techniques are often invasive and the effects of exogenous agents or genetic manipulation on the cell physiology are still unknown. An additional drawback is induced by the commonly desired high specificity of the labelling, as only the labelled parts of the cell contribute to the measurement, while the behavior of all other cell parts remains undetected. Hence, it is highly desirable to use non-invasive contrast-agent-free microscopy to study the dynamics and physiological activity of various structures in living cells, simultaneously.

In recent years the mechanical contrast has been identified to be an important biomarker for many biological processes [1–10]. Traditional approaches based on ultrasound or atomic force microscopy (AFM) rely on physical access to the sample [11,12]. AFM is often used as the reference due to the high spatial resolution it offers, but is not ideal for biomedical applications due to the low temporal resolution and the limitation to surface measurements.

Optical techniques are favorable as they are non-invasive/contactless. A particularly emerging optical measurement method able to perform three-dimensional non-contact high spatial resolution measurements on biological (also in vivo) samples, is spontaneous Brillouin microscopy (SB). Spontaneous Brillouin scattering microscopy utilizes the photon-phonon interaction of focused light with random thermal phonons [13]. In most cases a confocal setup is used where the back

#449980 https://doi.org/10.1364/OE.449980
Journal © 2022 Received 1 Dec 2021; revised 23 Dec 2021; accepted 27 Dec 2021; published 31 Jan 2022

Optics EXPRESS

scattered light is evaluated with sophisticated spectroscopic setups [14]. This allows spontaneous Brillouin scattering microscopy the contactless measurement of biological samples in subcellular resolution with relative uncertainties as low as 0.001 [15]. No material-changing treatment of the sample is required for the measurement. However, the signal generation process is very weak, which leads to long integration times for a single point measurement and prohibits the acquisition of dynamic behaviours.

To speed-up the acquisition, stimulated Brillouin scattering techniques were studied. Such techniques have especially been used for material characterization [16–19]. The advantage of the stimulated techniques is that due to the separation of excitation and readout, the signal-to-noise ratio (SNR) can, to a certain extent be manipulated by the excitation conditions, which promises a speed advantage compared to SB. The stimulation is done by coherently overlapping laser beams, which interfere in the sample and thereby stimulate phonons, in contrast to thermal phonons at spontaneous scattering. For readout a third, probing beam interacts with the stimulated region. In stimulated Brillouin scattering (SBS)-microscopy the light source used for excitation is a tunable continuous-wave (cw) laser [20–22]. Impulsive SBS (ISBS) [23,24] microscopy is based on the generation of a transient density grating via the interference of two ultra-short laser pulses .

In this paper we study the influence of the excitation pulse parameters on the resulting signal strength and achievable measurement rates. Measurements on hydrogels are performed, which can be considered as model materials for biological samples [25].

2. Experimental setup

The experimental setup is depicted in Fig. 1. For generation of ultrashort pulses a Coherent Monaco laser, that has a broad range of operation parameters and allows tuning repetition rate, pulse length and energy is used. All studies are performed at the wavelength of $\lambda = 517nm$. The pulsed light is focused onto the optical grating (GT). All but the plusmn 1st diffraction orders are blocked in the Fourier space between lenses L4 and L5. These form a 4f setup and image the grating into the region of interest (ROI). In the ROI the plusmn 1st diffraction orders of the excitation beam interfere. The resulting interference fringe pattern excites a time varying density grating, which comes along with a time varying refractive index change. The

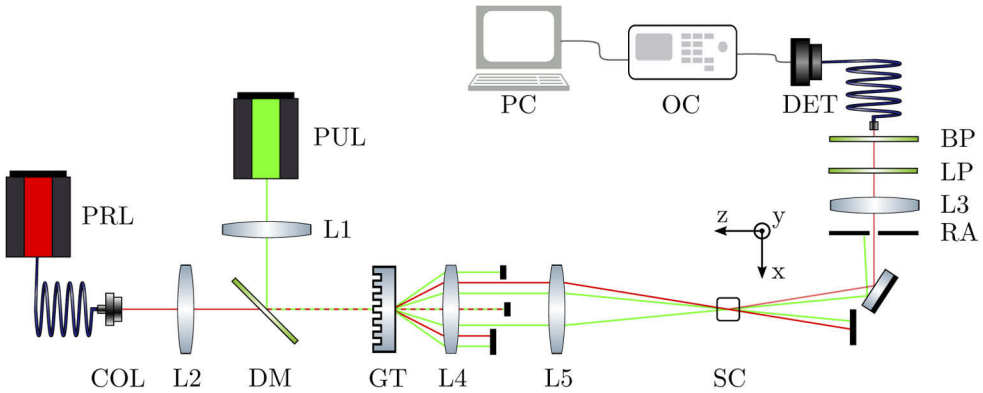

Fig. 1. ISBS microscope setup: PUL excitation laser (517 nm, Coherent Monaco); PRL probe laser (895 nm, DL100 Toptica Photonics); DM dichroic mirror (DMLP650 Thorlabs); COL collimator; L1 to L5 achromatic lenses (AC245-Series Thorlabs); GT grating (custom, grating constant 8 µm); SC sample container (Fused Quartz Cuvettes Thorlabs); RA rectangular aperture; LP long-pass (FEL0850 Thorlabs); BP band-pass (900/11 nm BrightLine Semrock); DET detector (APD, Femto Berlin); OC oscilloscope; PC personal computer.

Optics EXPRESS

fringe spacing of the time-varying grating is $d = \frac{\lambda}{2sin(\phi)}$, with the wavelength λ and crossing angle ϕ. The readout of the grating is achieved by Bragg-diffraction of a continuous wave probe laser. The readout beam is coupled into the setup employing dichroic optics and is also focused on GT. All but the -1st order of the probe beam are blocked. The remaining beam is Bragg-diffracted by the time-varying grating, which results in an intensity modulation. In this geometry the Bragg-condition is automatically fulfilled [24]. The Bragg-diffracted probe-beam is filtered with spatial and wavelength filters and is directed towards the detector. Evaluation of the modulation frequency of the Bragg-diffracted probe beam gives access to the speed of sound in the measurement volume and thus to the local mechanical properties.

3. Signal components

The signal generation processes involved in ISBS are shown in Fig. 2. The interference fringe system is translated into an acoustic wave by thermal and electrostrictive effects. While thermal effects are induced by absorption of the pump laser interference fringe system, electrostrictive effects are created by locally induced displacement of matter in the direction of the regions with high light intensity [26]. A higher polarizability of the medium increases the electrostrictive excitation. The electric field E of the Bragg-diffracted part of the probe beam can be described as follows:

$$E = T\left(1 - \cos(\omega t)\cdot \mathrm{e}^{-\alpha t}\right) - S\sin(\omega t)\cdot \mathrm{e}^{-\alpha t} \tag{1}$$

where T and S represent the amplitude of the thermal and electrostrictive components, respectively. ω is the angular frequency of the oscillation which results from $\omega = (2\pi v)/d$, with the speed of sound v [27]. The refractivity of the grating is not only oscillatory as in Eq. 1 but also damped. This damping arises, on the one hand, from the divergence of the two sound components propagating in opposite directions and the damping of the sound in the sample. This is represented by the attenuation coefficient α. The resulting intensity I on the detector is thus directly proportional to the time-averaged amplitude of the electric field squared $I \propto \left\langle |\underline{E}|^2 \right\rangle$. Thus it follows:

$$\begin{aligned} I \propto\ & T^2 + \mathrm{e}^{-\alpha t}\left(-2ST\sin(\omega t) - 2T^2\cos(\omega t)\right) \\ & + \mathrm{e}^{-2\alpha t}\left(0.5S^2 + 0.5T^2 - 0.5S^2\cos(2\omega t) + 0.5T^2\cos(2\omega t)\right. \\ & \left. +\ ST\sin(2\omega t)\right). \end{aligned} \tag{2}$$

Equation 2 shows that the signal consists of components that oscillate with different frequencies. The double frequency $2f$ components decay faster than components that oscillate with the single frequency. Furthermore, the oscillation with purely $2f$ is exclusively due to electrostrictive excitation, while when thermal effects are present, both $f_1 = f$ and $f_2 = 2f$ appear. Exemplary simulated time signals for pure thermal (T), pure electrostrictive (S) and both, thermal and electrostrictive, are plotted in Fig. 3. Parts of the readout beam that are not Bragg-diffracted by the grating, but scattered in the beam path, e.g. in the sample can coherently overlap on the detector, leading to a homodyne detection of frequency f. The desired information is contained in both f and $2f$. However, a large contribution of thermal excitation means a high energy deposition and is thus an indicator for phototoxicity. In conclusion, electrostrictive excitation can be beneficial.

Optics EXPRESS

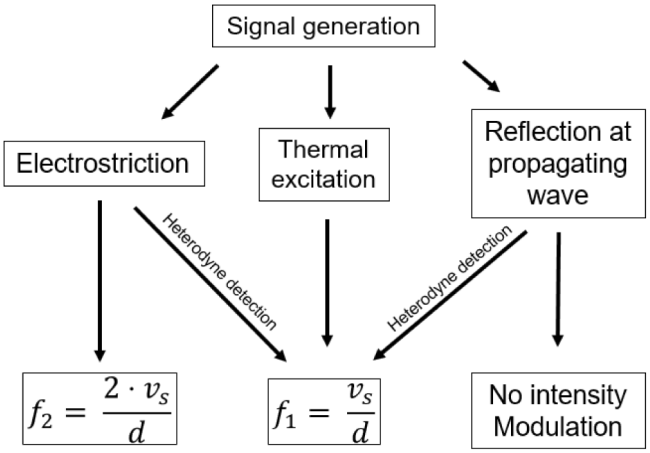

Fig. 2. The signal generation processes of ISBS. The intensity modulation of the probe beam is proportional to the local speed of sound v_s, which is linked to the mechanical properties. The oscillation takes place with two modulation frequencies f_1 and $f_2 = 2f_1$, that depend on the dominant generation process.

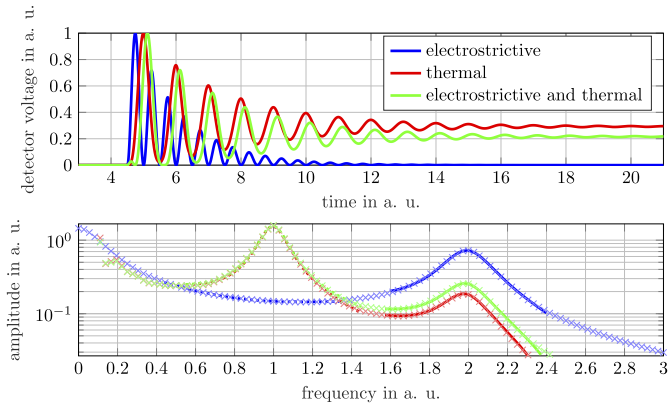

Fig. 3. Simulated signals for the electrostrictive, thermal and combined excitation regime.

4. Measurements of methanol

The influence of different excitation parameters on the ISBS signal-strength was experimentally determined. As a measure of the signal-strength we use fitting and integration of the signal in the frequency domain, see Fig. 4..

In an ideal system, with maximum detection sensitivity and high SNRs, single-shot detection would be possible. However, in real-life experiments the sensitivity and signal-strength are limited. To increase the SNR, averaging can be used, which goes with $SNR \propto \sqrt{N}$ according to Poisson statistics. However, the exposure time T increases linearly with the number of averaged signals $T = \frac{N}{f_p}$.

The damage-threshold of the specimen gives an upper bound on the usable light-dose, which is the sum power density of the average deposited power of the pulsed excitation of the pump laser and the cw-readout power of the probe laser. In order to exploit the potential speed advantage of ISBS over SB, the measurement has to come along with the minimum possible number of signal averaging, which requires the highest possible SNR values. The SNR of the ISBS signal is

Optics EXPRESS

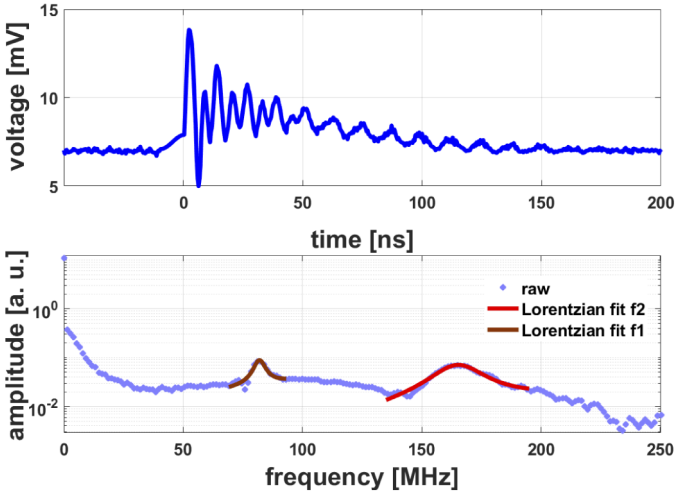

Fig. 4. Typical time-signal and corresponding Fourier spectrum.

directly linked to the readout power and the visibility of the transient refractive index grating Δn, which can be optimized by the choice of the excitation parameters. The most important parameter is the excitation pulse energy, which changes both the average and the peak power. Employing a finite element method based simulation for the thermal induced grating, we obtain a quadratic dependency between increasing excitation pulse energy and the maximum induced refractive index change, shown in Fig. 5.

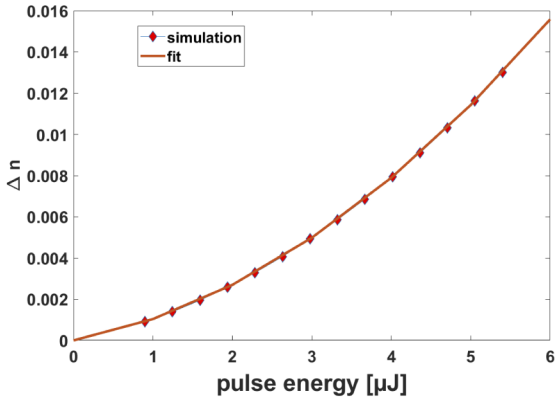

Fig. 5. A finite element simulation of the ISBS excitation in water shows a quadratic increase of the modulation depth Δn with increasing excitation pulse energy. Here just the thermal excitation with $f_1 = f$ is considered.

This behaviour is validated experimentally. Increasing the excitation-pulse-energy at constant repetition rate of 1 kHz and pulse-length of 2 ps, leads to a non-linear increase of the signal amplitude (Fig. 6(a)) for both frequencies f_1 and $f_2 = 2f_1$, at an averaging of N=100*512. Increasing the power of the probe beam instead just leads to a linear increase of the signal amplitude (see Fig. 7).

Hence it is advantageous to work at higher excitation energies instead of higher readout powers. The average excitation power was $P_{ave} \leq 10$ mW. The power of the readout beam was set to approximately $P_{read} = 28$ mW. Increased signal amplitude additionally reduce the statistical

Optics EXPRESS

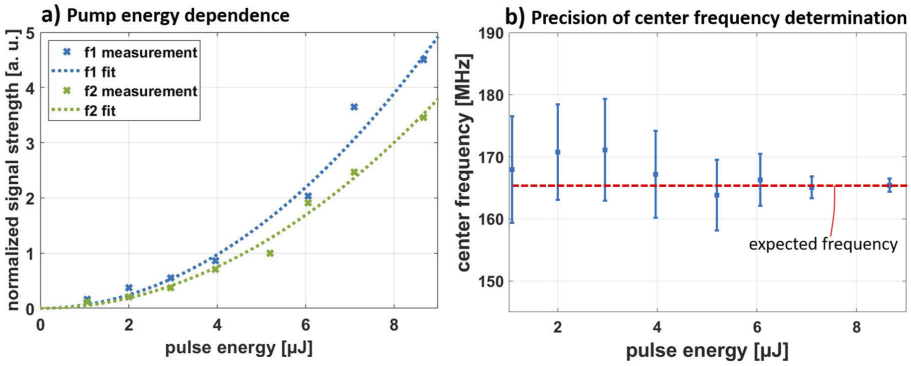

Fig. 6. a) Pulse energy dependent, normalized ISBS signal measured in methanol. The connection between the signal strength of the oscillations of both f and $2f$ and the excitation energy is non-linear. The pulse-length was set to 2 ps and the repetition rate was 1 kHz at N=100*512 averages. The maximum used average excitation power in this measurement was 10 mW. The coefficient of determination for a plain quadratic function is R = 0.95 and R = 0.99 for f and $2f$ respectively. b) The precision of the determination of the Brillouin frequency increases with increasing excitation energy. Here the evaluation was done with 10 signals of N=10*512 averages for the signal of frequency f_2. The error bars display the standard deviation of the measurements.

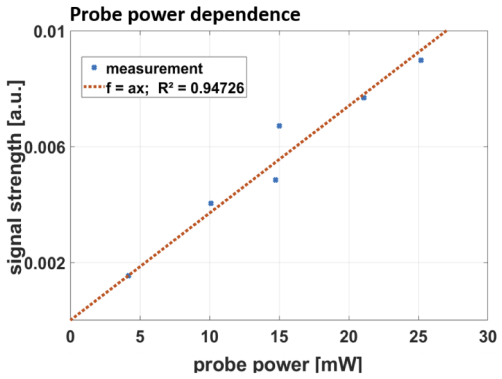

Fig. 7. The signal strength increases linearly with the probe power.

error of the measurement, as the uncertainty of the Brillouin frequency determination is reduced (Fig. (6(b)).

In theory, the optimal repetition rate is given by the decay time of the acoustic wave. Once the medium has reached the equilibrium state, the next excitation pulse can follow. The decay time also depends on the size of the measurement volume. In the configuration described in the paper the measured decay time is in the range of 100 ns. Hence, in an ideal system the maximum repetition rate could reach up to 10 MHz. However, it has to be considered that the time-varying grating has a time varying diffraction efficiency, which at some point will drop below the sensitivity-level of the system. Hence, the measured decay-time will be underestimated and a reduced repetition-rate compared to the calculated one has to be used. To separate the influence of the average deposited power from the peak powers, we chose a constant energy per pulse of 5 µJ (2 ps, N=512*100) and increased the repetition rate from 100 Hz to 750 kHz, which means that the average deposited power is increased. We observe a change of the signal

Optics EXPRESS

composition, however the signal strength is constant over a large range but drops towards the high used rates. At low rates mainly electrostriction contributes to the signal. From a repetition rate of 2 kHz, i.e. an average power of $P_{ave1} = 10$ mW, the influence of the thermal grating starts to become pronounced. At 100 kHz, i.e. $P_{ave2} = 500$ mW, the strength of the thermal grating is larger than the electrostrictive component (Fig. 8 and Fig. 9). This means that the risk for photodamage strongly increases, which however is actually strongly dependent on the light wavelength. The corresponding power densities are $P_{dens1} = 200\frac{W}{cm^2}$ and $P_{dens2} = 10000\frac{W}{cm^2}$. The power density of the cw readout is calculated to be $P_{read} = 560\frac{W}{cm^2}$. These values in general are still adequate, as typical optical power densities used for other Brillouin approaches are higher due to the smaller foci used. For spontaneous Brillouin typical values are in the range of $P_{SB}>10^5\frac{W}{cm^2}$ [28] and for cw-stimulated Brillouin-scattering $P_{SBS}>10^7\frac{W}{cm^2}$, at 780 nm [22],

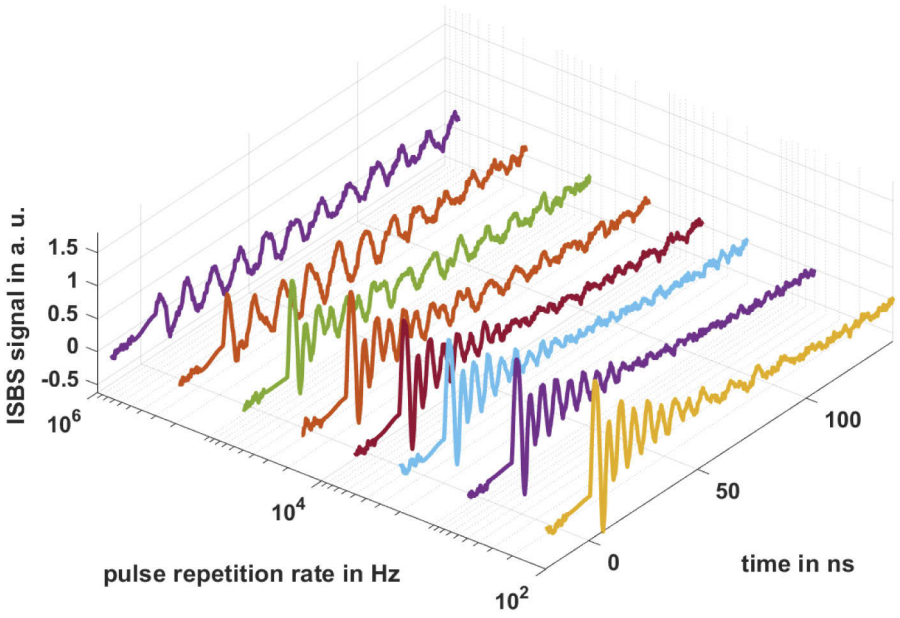

Fig. 8. Measurement of methanol. At low pulse repetition rates the signal consists of pure electrostriction. Increasing the repetition rate at constant pulse energy, i.e. increasing the average deposited power, increases the influence of the thermal grating, leading to a change of the intensity modulation frequency from f_2 to f_1. With this change, the main signal comes from a thermal grating, which leads to an increased decay-time.

Furthermore, the observable decay time increases with the influence of the thermal grating, which is in agreement with Eq. (2).

For the choice of the pulse-length it is just important that the excitation is impulsive, which means that the periode length of the accoustic oscillaction has to be significantly longer then the pulse length. We could not observe an influence of changing the pulse length from 500 fs to 10 ps at constant energies on the signal amplitude. Comparable observations were reported in [29]. From the measurements above we can derive as a consequence, that the main parameter for increasing the signal amplitude is the used excitation pulse energy, which directly influences the peak power. An increase of the average power does not improve the signal, but increases the heating of the sample. Decreasing the measurement volume size, which is desired to improve the spatial resolution, requires a reduction of the pulse energy and the repetition rate, which strongly affects the signal amplitude. This means that a sample- and setup- dependent balance of the excitation parameters has to be found.

Optics EXPRESS

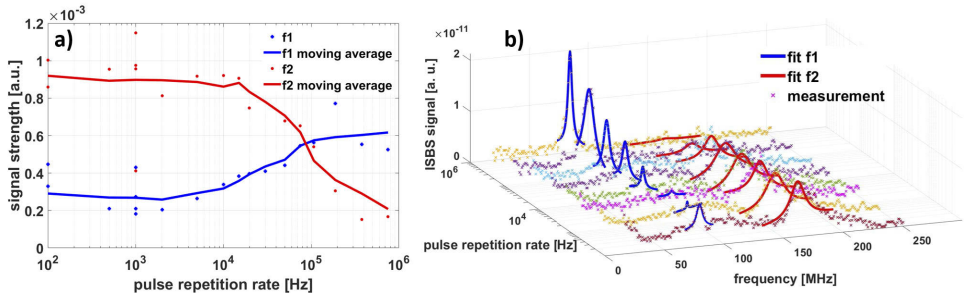

Fig. 9. Measurement of methanol. a) Signal strength of f_1 and f_2. The signal-composition changes with deposited power. At low average power the main contributor is electrostriction. From approx. $10mW$ the signal amplitude of f_2 deteriorates, while f_2 strengthens. b) Corresponding Fourier spectra.

5. Measurements on polyacrylamide-hydrogels

The biologically relevant polyacrylamide-hydrogels, that have already been used in [24], can be employed as a reference sample to extract the feasible excitation parameters of the system shown in Fig. 1. A first big difference to the measurement on methanol is that we just observe f_1. This suggests that the absorption in the hydrogel is much stronger than in methanol (compare Fig. 10).

Figure 11 shows excitation energy dependent measurements. For each excitation pulse energy we recorded N=512*60 signals. These measurements are used to determine how many averages are required to reduce the standard deviation of the determination of the Brillouin frequency to obtain a qualitatively good measurement. A relative precision of 0.3 – 0.7% is the typical range for systems operating with impulsive stimulated, cw-stimulated and spontaneous Brillouin scattering [30].

At an excitation pulse energy of 8.75 µJ just N=10 averages were required to achieve a relative precision of 0.7%, which corresponds to an acquisition time for a single-point measurement of $T_{min} \approx 0.3ms$ (Fig. 12). An increased precision of 0.3% is achieved at N=120 averages, which takes 3.6 ms. Reducing the excitation pulse energy, increases the required number of averages

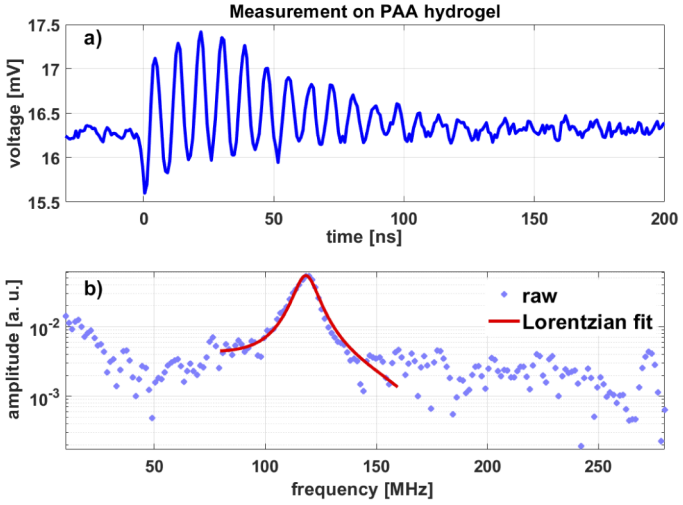

Fig. 10. a) Exemplary time signal and b) corresponding Fourier spectrum.

Optics EXPRESS

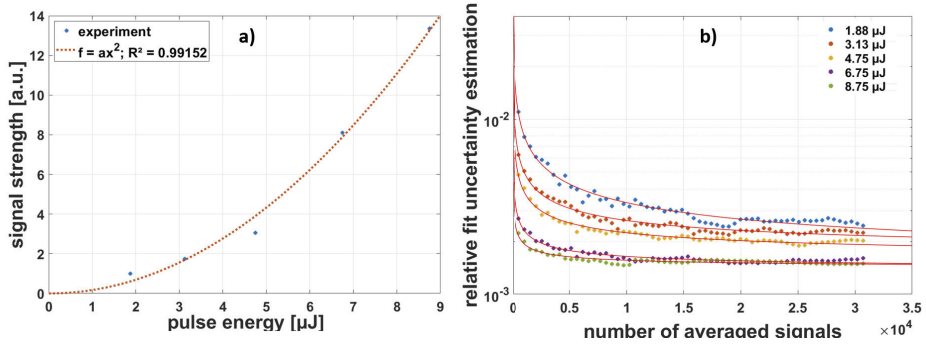

Fig. 11. a) Excitation-energy dependent measurement on polyacrylamide-hydrogels. b) The number of required averages to obtain a low uncertainty decreases with increasing pulse energy. The required number of averages limits the achievable measurement rate and decreases with the excitation energy.

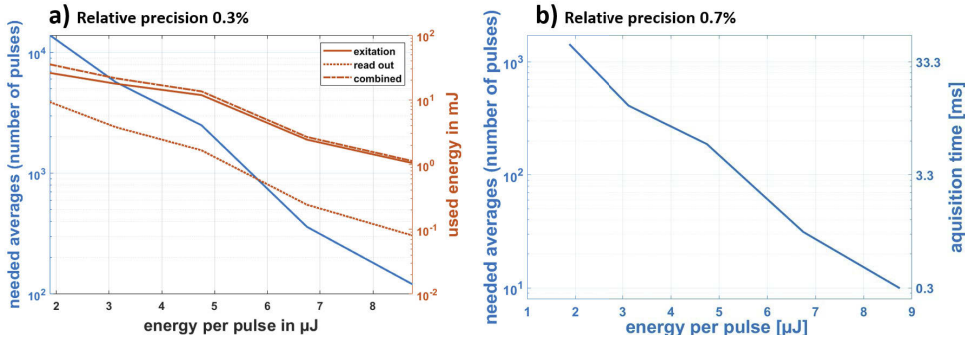

Fig. 12. a) Required number of averages to reach 0.3% precision. b) Point measurements at an acquisition time of 0.3 ms are possible, with only N=10 averages at 8.75 µJ excitation pulse energy.

and thus the acquisition time. Increasing the pulse energy comes with the danger of photodamage, but improves signal-strength, lowers the required averages and thus reduces the acquisition-time.

6. Discussion and conclusion

Impulsive stimulated Brillouin microscopy has the potential to achieve high-speed measurements of viscoelastic properties. The main parameter that improves the signal-strength is the pulse energy, i.e. the peak-power. The results show that ISBS can be a very fast alternative to SB. However, it can also be concluded, that it is a narrow sample-dependent set of parameters that allows to exploit the full potential of ISBS. From the maximum allowed pulse energy the minimum required averages for a targeted precision can be derived, which places a limit to the sample-dependent achievable point measurement rate. It has to be noted that above mentioned studies are conducted for a wavelength of $\lambda = 517nm$. Beside the laser parameters, the sensitivity of the detection system is a further key to improve. Assuming maximum system sensitivity the point-measurement rate is theoretically limited by the decay time of the acoustic wave. A transfer of ISBS to clinical applications requires an increase of the spatial resolution by decreasing the size of the measurement volume. According to Figs. 4 and 8, Brillouin signals in electrostrictive regime are typically around 100 ns, however also signal durations of 25 ns were observed. Assuming durations of 100 ns and N=1000 averages would result in a point-measurement rate

Optics EXPRESS

of 10 kHz with acquisition time of 0.1 ms. At this rate, the introduction of lateral scanning would enable to measure an image of 500 pixel with video-rate (20 Hz). However, the discussion of phototoxicity and other constraints have to be taken into account, see the chapters 4 and 5. Employing adaptive optical approaches [31–33] could further extent the applicabity of the system to scattering environments. Furthermore, fiber technology can enable minimally invasive Brillouin endomicroscopy [34–36]. With the adequate choice of the excitation parameters, ISBS promises to achieve high-speed mapping of viscoelastic properties of biological samples.

Funding. Deutsche Forschungsgemeinschaft (Cz55/44-1).

Acknowledgments. The authors would like to thank Raimund Schlüßler (Biotechnology Center, TU Dresden). Furthermore we gratefully acknowledge the valuable contributions of Fabian Rottmann on Comsol simulations.

Disclosures. The authors declare that there are no conflicts of interest related to this article.

Data availability. Data are available from the authors upon reasonable request.

References

1. A. Sarvazyan, T. J. Hall, M. W. Urban, M. Fatemi, S. R. Aglyamov, and B. S. Garra, "An overview of elastography - an emerging branch of medical imaging," Curr. Med. Imaging Rev. **7**(4), 255–282 (2011).
2. G. Y. H. Lee and C. T. Lim, "Biomechanics approaches to studying human diseases," Trends Biotechnol. **25**(3), 111–118 (2007).
3. K. V. Larin and D. D. Sampson, "Optical coherence elastography - OCT at work in tissue biomechanics [invited]," Biomed. Opt. Express **8**(2), 1172–1202 (2017).
4. R. Muthupillai, D. J. Lomas, P. J. Rossman, J. F. Greenleaf, A. Manduca, and R. L. Ehman, "Magnetic resonance elastography by direct visualization of propagating acoustic strain waves," Science **269**(5232), 1854–1857 (1995).
5. D. Claus, M. Mlikota, J. Geibel, T. Reichenbach, G. Pedrini, J. Mischinger, S. Schmauder, and W. Osten, "Large-field-of-view optical elastography using digital image correlation for biological soft tissue investigation," J. Med. Imag **4**(1), 014505 (2017).
6. K. D. Mohan and A. L. Oldenburg, "Elastography of soft materials and tissues by holographic imaging of surface acoustic waves," Opt. Express **20**(17), 18887–18897 (2012).
7. O. Otto, P. Rosendahl, A. Mietke, S. Golfier, C. Herold, D. Klaue, S. Girardo, S. Pagliara, A. Ekpenyong, A. Jacobi, M. Wobus, N. Töpfner, U. F. Keyser, J. Mansfeld, E. Fischer-Friedrich, and J. Guck, "Real-time deformability cytometry: on-the-fly cell mechanical phenotyping," Nat. Methods **12**(3), 199–202 (2015).
8. J. A. Mulligan, X. Feng, and S. G. Adie, "Quantitative reconstruction of time-varying 3d cell forces with traction force optical coherence microscopy," Sci. Rep. **9**(1), 4086 (2019).
9. N. Toepfner, C. Herold, O. Otto, P. Rosendahl, A. Jacobi, M. Kräter, J. Stächele, L. Menschner, M. Herbig, L. Ciuffreda, L. Ranford-Cartwright, M. Grzybek, Ü. Coskun, E. Reithuber, G. Garriss, P. Mellroth, B. Henriques-Normark, N. Tregay, M. Suttorp, M. Bornhäuser, E. R. Chilvers, R. Berner, and J. Guck, "Detection of human disease conditions by single-cell morpho-rheological phenotyping of blood," eLife **7**, e29213 (2018).
10. R. W. Sanderson, A. Curatolo, P. Wijesinghe, L. Chin, and B. F. Kennedy, "Finger-mounted quantitative micro-elastography," Biomed. Opt. Express **10**(4), 1760–1773 (2019).
11. C. L. de Korte, G. Pasterkamp, A. F. W. van der Steen, H. A. Woutman, and N. Bom, "Characterization of plaque components with intravascular ultrasound elastography in human femoral and coronary arteries in vitro," Circulation **102**(6), 617–623 (2000).
12. H. O. B. Gautier, A. J. Thompson, S. Achouri, D. E. Koser, K. Holtzmann, E. Moeendarbary, and K. Franze, "Atomic force microscopy-based force measurements on animal cells and tissues," in *Methods in Cell Biology*, vol. 125 of *Biophysical Methods in Cell Biology* , (eds.) (Academic Press, 2015), pp. 211–235.
13. Z. Meng, A. J. Traverso, C. W. Ballmann, M. A. Troyanova-Wood, and V. V. Yakovlev, "Seeing cells in a new light: a renaissance of Brillouin spectroscopy," Adv. Opt. Photonics **8**(2), 300–327 (2016).
14. G. Scarcelli and S. H. Yun, "Confocal Brillouin microscopy for three-dimensional mechanical imaging," Nat. Photonics **2**(1), 39–43 (2008).
15. G. Antonacci, T. Beck, A. Bilenca, J. Czarske, K. Elsayad, J. Guck, K. Kim, B. Krug, F. Palombo, R. Prevedel, and G. Scarcelli, "Recent progress and current opinions in Brillouin microscopy for life science applications," Biophys. Rev. **12**(3), 615–624 (2020).
16. M. S. Brown, Y. Li, W. L. Roberts, and J. R. Gord, "Analysis of transient-grating signals for reacting-flow applications," Appl. Opt. **42**(3), 566–578 (2003).
17. S. Schlamp, T. Rosgen, D. N. Kozlov, C. Rakut, P. Kasal, and J. von Wolfersdorf, "Transient grating spectroscopy in a hot turbulent compressible free jet," J. Propul. Power **21**(6), 1008–1018 (2005).
18. F. Bencivenga, R. Mincigrucci, F. Capotondi, L. Foglia, D. Naumenko, A. A. Maznev, E. Pedersoli, A. Simoncig, F. Caporaletti, V. Chiloyan, R. Cucini, F. Dallari, R. A. Duncan, T. D. Frazer, G. Gaio, A. Gessini, L. Giannessi, S. Huberman, H. Kapteyn, J. Knobloch, G. Kurdi, N. Mahne, M. Manfredda, A. Martinelli, M. Murnane, E. Principi, L. Raimondi, S. Spampinati, C. Spezzani, M. Trovò, M. Zangrando, G. Chen, G. Monaco, K. A. Nelson, and C.

Optics EXPRESS

Masciovecchio, "Nanoscale transient gratings excited and probed by extreme ultraviolet femtosecond pulses," Sci. Adv. **5**(7), eaaw5805 (2019).
19. J. Czarske and H. Müller, "Heterodyne detection technique using stimulated brillouin scattering and a multimode laser," Opt. Lett. **19**(19), 1589–1591 (1994).
20. C. W. Ballmann, J. V. Thompson, A. J. Traverso, Z. Meng, M. O. Scully, and V. V. Yakovlev, "Stimulated brillouin scattering microscopic imaging," Sci. Rep. **5**(1), 18139 (2015).
21. I. Remer and A. Bilenca, "Background-free brillouin spectroscopy in scattering media at 780 nm via stimulated brillouin scattering," Opt. Lett. **41**(5), 926–929 (2016).
22. I. Remer, R. Shaashoua, N. Shemesh, A. Ben-Zvi, and A. Bilenca, "High-sensitivity and high-specificity biomechanical imaging by stimulated brillouin scattering microscopy," Nat. Methods **17**(9), 913–916 (2020).
23. C. W. Ballmann, Z. Meng, A. J. Traverso, M. O. Scully, and V. V. Yakovlev, "Impulsive brillouin microscopy," Optica **4**(1), 124–128 (2017).
24. B. Krug, N. Koukourakis, and J. W. Czarske, "Impulsive stimulated Brillouin microscopy for non-contact, fast mechanical investigations of hydrogels," Opt. Express **27**(19), 26910–26923 (2019).
25. M. Bailey, M. Alunni-Cardinali, N. Correa, S. Caponi, T. Holsgrove, H. Barr, N. Stone, C. P. Winlove, D. Fioretto, and F. Palombo, "Viscoelastic properties of biopolymer hydrogels determined by brillouin spectroscopy: A probe of tissue micromechanics," Sci. Adv. **6**(44), eabc1937 (2020).
26. D. C. Lamb, G. C. Lin, and A. G. Doukas, "Picosecond grating spectroscopy for characterizing the acoustic properties of biological material," Appl. Opt. **36**(7), 1660–1666 (1997).
27. M. Fayer, "Picosecond holographic grating generation of ultrasonic waves," IEEE J. Quantum Electron. **22**(8), 1437–1452 (1986).
28. M. Nikolić and G. Scarcelli, "Long-term brillouin imaging of live cells with reduced absorption-mediated damage at 660nm wavelength," Biomed. Opt. Express **10**(4), 1567–1580 (2019).
29. C. W. Ballmann, Z. Meng, and V. V. Yakovlev, "Nonlinear brillouin spectroscopy: what makes it a better tool for biological viscoelastic measurements," Biomed. Opt. Express **10**(4), 1750–1759 (2019).
30. R. Schlüßler, S. Möllmert, S. Abuhattum, G. Cojoc, P. Müller, K. Kim, C. Möckel, C. Zimmermann, J. Czarske, and J. Guck, "Mechanical mapping of spinal cord growth and repair in living zebrafish larvae by brillouin imaging," Biophys. J. **115**(5), 911–923 (2018).
31. N. Koukourakis, B. Fregin, J. König, L. Büttner, and J. W. Czarske, "Wavefront shaping for imaging-based flow velocity measurements through distortions using a fresnel guide star," Opt. Express **24**(19), 22074–22087 (2016).
32. K. Philipp, F. Lemke, S. Scholz, U. Wallrabe, M. Wapler, N. Koukourakis, and J. Czarske, "Diffraction-limited axial scanning in thick biological tissue with an aberration-correcting adaptive lens," Sci. Rep. **9**(1), 9532 (2019).
33. L. Büttner, M. Thümmler, and J. Czarske, "Velocity measurements with structured light transmitted through a multimode optical fiber using digital optical phase conjugation," Opt. Express **28**(6), 8064–8075 (2020).
34. J. Czarske, "A miniaturized dual-fibre laser doppler sensor," Meas. Sci. Technol. **12**(8), 1191–1198 (2001).
35. E. Scharf, J. Dremel, R. Kuschmierz, and J. Czarske, "Video-rate lensless endoscope with self-calibration using wavefront shaping," Opt. Lett. **45**(13), 3629–3632 (2020).
36. Y. Xiang, C. Basirun, J. Chou, M. E. Warkiani, P. Török, Y. Wang, S. Gao, and I. V. Kabakova, "Background-free fibre optic brillouin probe for remote mapping of micromechanics," Biomed. Opt. Express **11**(11), 6687–6698 (2020).